

$N - 2$) and those of the odd numbers were set to be $g_n = \exp(j\alpha)$ ($n = 1, 3, \dots, N - 1$). The output power of the transversal filter is given from eqn. 1 by

$$T = |G|^2 = \left| \frac{1}{N} (1 + e^{j\alpha}) \times \frac{N}{2} \right|^2 = |\cos(\alpha/2)|^2 \quad (2)$$

Fig. 2 compares the experimental normalised output power with the theoretical output power given by eqn. 2. The circles represent the experimental values for $\alpha = 0, \pi/3, \pi/2, 2\pi/3$ and π . It is confirmed that the collective summation of complex electric fields is obtainable by using an MMI combiner. The fibre-to-fibre insertion loss at zero phase variation was 5.6dB. There are several loss origins; they are, a 0.4dB theoretical loss in each MMI splitter and combiner, a 0.1dB theoretical loss in the MMI 3dB coupler, a 0.06dB intersecting waveguide loss for each intersection [6] and a 0.1dB coupling loss in the dispersion shifted fibre. When we sum up these losses, we have a $0.4(\text{dB}) \times 2$ (MMI splitter and combiner) + $0.1(\text{dB}) \times 2$ (MMI 3dB couplers) + $0.06(\text{dB}) \times 15$ (intersections) + $0.1(\text{dB}) \times 2$ (facets) = 2.1 (dB) loss without including the waveguide propagation loss. The total waveguide length of the transversal filter is $\sim 27\text{cm}$. If we assume a reasonable waveguide loss of 0.13dB/cm , the total waveguide propagation loss becomes 3.5dB. The above loss breakdown sums up to $2.1 + 3.5 = 5.6(\text{dB})$ which agrees with the experimental value. When we exclude the 3.5dB waveguide loss and 0.2dB fibre coupling losses, the inherent loss of the transversal filter is evaluated to be $\sim 1.9\text{dB}$.

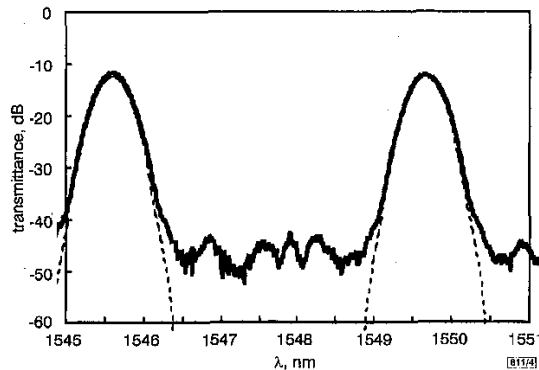


Fig. 4 Spectral intensity transmittances of filter when g_n has Gaussian profile

— experimental values
- - - theoretical values

To confirm the signal processing capabilities, sinc-type and Gaussian-type spectral filter responses have been synthesised. Fig. 3 shows the spectral transmittances of the filter when $g_n = 1$ for all n . Since the functional shape of g_n and the spectral transmittance G are connected by a Fourier transform relationship, the theoretical intensity transmittance is expressed by

$$T = |G|^2 = \left| \frac{\sin(N\phi/2)}{N \sin(\phi/2)} \right|^2 \quad (3)$$

where $\phi = (2\pi n_i/\lambda)\Delta L = 2\pi f/FSR$ and f denotes the optical frequency. The peak transmittance is -5.6dB . Fig. 4 shows the spectral transmittances of the filter when g_n has the following Gaussian profile:

$$g_n = \exp \left[-\frac{(n-7)(n-8)}{16} \right] \quad (n = 0, 1, \dots, 15) \quad (4)$$

The theoretical intensity transmittance also has Gaussian shape as shown by the dotted line in Fig. 4. The peak transmittance becomes -12dB . An additional loss of 6.4dB is caused by cutting out the signal power in each tap arm to form Gaussian tap coefficients. It is shown from Figs. 3 and 4 that an arbitrary shape of the filter characteristics can be realised by the present transversal filter.

Conclusion: The fabrication of a fully integrated coherent optical transversal filter has been reported. It is confirmed that the collective summation of complex electric fields is obtainable by using an

MMI combiner. Programmable spectral filters and chromatic dispersion equalisers can be realised by using the presented transversal filter. Experiments are now in progress and the results will be reported in the future.

Acknowledgments: The authors would like to thank members of the Okamoto Research Laboratory and Hyper-Photonic Component Laboratory for their co-operation.

© IEE 1999

Electronics Letters Online No: 19990940
DOI: 10.1049/el:19990940

22 June 1999

K. Okamoto, H. Yamada and T. Goh (NTT Photonics Laboratories, 162 Tokai, Naka-gun, Ibaraki, 319-11, Japan)

E-mail: okamoto@iba.iecl.ntt.jp

References

- JACKSON, K.P., NEWTON, S.A., MOSLEHI, B., CUTLER, M.C.C., GOODMAN, J.W., and SHAW, H.J.: 'Optical fiber delay-line signal processing', *IEEE Trans.*, 1985, **MTT-33**, pp. 193-210
- SASAYAMA, K., OKUNO, M., and HABARA, K.: 'Photonic FDM multichannel selector using coherent optical transversal filter', *IEEE J. Lightwave Technol.*, 1994, **LT-12**, pp. 664-669
- TAKIGUCHI, K., JINGUI, K., and OHMORI, Y.: 'Variable group-delay dispersion equaliser based on a lattice-form programmable optical filter', *Electron. Lett.*, 1995, **31**, pp. 1240-1241
- TAKIGUCHI, K., JINGUI, K., OKAMOTO, K., and OHMORI, Y.: 'Variable group-delay dispersion equalizer using lattice-form programmable optical filter on planar lightwave circuit', *IEEE J. Sel. Topics Quantum Electron.*, 1996, **QE-2**, pp. 270-276
- SOLDANO, L.B., and PENNINGS, C.M.: 'Optical multi-mode interference devices based on self-imaging: principles and applications', *IEEE J. Lightwave Technol.*, 1995, **LT-13**, pp. 615-627
- KOMINATO, T., KITO, T., KATO, K., HIBINO, Y., and YASU, M.: 'Loss characteristics of intersecting silica-based waveguides', *Optoelectronics Conf. OEC'92*, 1992, Paper 16B4-1, pp. 138-139
- HIDA, Y., HIBINO, Y., OKAZAKI, H., and OHMORI, Y.: '10-m long silica-based waveguide with a loss of 1.7dB/m ', *IPR'95*, Dana Point, CA, 1995, Paper 1ThC6

Grating formation in BGG31 glass by UV exposure

D. Provenzano, W.K. Marshall, A. Yariv,
D.F. Geraghty, S. Honkanen and N. Peyghambarian

A three-dimensional index variation grating in bulk BGG31 glass written using neither hydrogen loading nor germanium doping is demonstrated. This material is useful for fabricating ion-exchanged waveguides, and its photosensitivity to ultraviolet (UV) radiation at 248nm has not been previously explored. Intensity measurements of the Bragg diffracted spots indicated a maximum index variation (Δn) of $\sim 4 \times 10^{-5}$.

Introduction: The field of optical communications has recently experienced a host of new devices to allow for higher bit rates. One area of innovation has been in the research of ion-exchanged waveguides [1], and incorporating Bragg gratings into such devices could lead to a great range of applications. Permanent index changes for gratings written in Ge-SiO_2 glasses have been reported [2]. Photobleaching has also been performed in a K^+ -exchanged waveguide with the 351nm line from an Ar^+ laser [3]. However, the photosensitivity was reportedly obtained by γ -ray irradiation pretreatment. In the waveguide material discussed in this Letter, there are no Ge-dopants [4] and no pretreatment of any kind, including hydrogen loading, thus allowing easier and cheaper fabrication.

We report the writing of a diffraction grating in a 2mm thick glass sample used for making Ag^+ ion-exchanged waveguides by exposure to radiation from a 248nm KrF excimer laser, without germanium doping nor hydrogen loading. BGG31 is a glass of the system $\text{SiO}_2/\text{B}_2\text{O}_3/\text{Al}_2\text{O}_3/\text{Na}_2\text{O}/\text{F}$, with $12.5\text{mol}\text{Na}_2\text{O}$. The three-dimensionally written gratings are evidence that neither germa-

nium nor hydrogen need be present to produce a reasonable index change with 248nm irradiation. The effect of the excimer exposure on the transmission of the glass can be seen in Fig. 1. Shown is the transmission against wavelength characteristics with and without exposure (no grating) and compared to a standard Corning glass microscope slide. The microscope slide transmission curve was unaffected by the excimer laser. Photobleaching the BGG31 glass with 248nm radiation changes the absorption spectrum near 350nm and appears to add a new absorption band near 520nm, with no noticeable differences above 650nm.

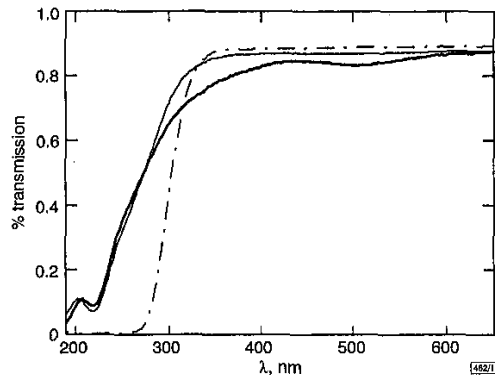


Fig. 1 Transmission spectrum for exposed and unexposed samples of BGG31 glass

— microscope slide
— BGG31 glass unexposed
— BGG31 glass exposed

For the grating inscription, the BGG31 glass sample was placed directly under a phase mask with a pitch of 1049.28nm (IBSEN Micro Structures A/S) and exposed with the excimer laser at 248nm (Lambda Physik Compex 110). For best results, the glass was placed in direct contact with the phase mask and exposed for 10min with 0.84J/cm² per pulse at 50Hz over an area of 2cm × 2mm. The beam was collimated in the long dimension (perpendicular to the phase mask rulings) and slightly focused in the short dimension. Other trials were carried out with gaps of 125 and 250μm between the phase mask and the sample, but in each case the diffraction spots from the Ar⁺ laser probe were reduced in intensity. This is consistent with reports [5, 6] that it is not the temporal coherence that limits the fringe visibility with mask/glass (or fibre) separation, but the spatial coherence.

The diffraction orders from the phase mask obey the equation

$$\Lambda_{mask} \sin \theta_m = m\lambda \quad (1)$$

where m is the diffracted order, $\lambda = 248\text{nm}$, and Λ_{mask} is the mask period = 1049.28nm. Each pair of beams produces an index variation grating in the material with a unique angle ϕ . Fig. 2 shows an example of a grating produced with the $-2, +1$ orders. The angle ϕ for a given grating is determined as the bisector of the angle between the propagation directions of any two orders, denoted m_1 and m_2 . The ± 1 orders produce gratings with $\phi = 0$, as will the ± 2 orders. α is the Bragg angle, measured as the angle of the incident (or reflected) ray with the tangent to the grating lines.

Characterisation of the written gratings was accomplished by probing these gratings with the 476nm line from an Ar⁺ laser operating at ~50mW. Evidence for a volume grating was that a very precise incident angle θ_{in} was needed to observe Bragg diffraction (Fig. 2). If only surface gratings had been produced by the excimer laser, then Bragg diffraction would have occurred at a continuum of angles. The Bragg condition for these photowritten gratings is

$$2 \left[\frac{\Lambda_{mask}}{m_1 - m_2} \cos \phi \right] \sin \alpha = m\lambda \quad (2)$$

where the term in brackets is the actual period of the desired grating, derived from the intensity distribution of any two diffracted orders m_1 and m_2 . m is the diffraction order from the probe, and here λ is 476nm. θ_{in} and θ_{out} can be obtained from α in eqn. 2 and account for the background material index of 1.4.

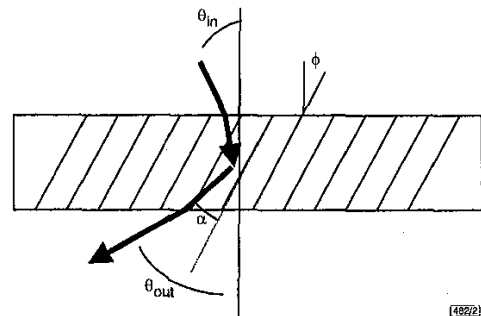


Fig. 2 Bragg diffraction from one of induced volume gratings

Probing was performed with 476nm line from Ar⁺ laser
Parallel lines show induced index-variation volume hologram

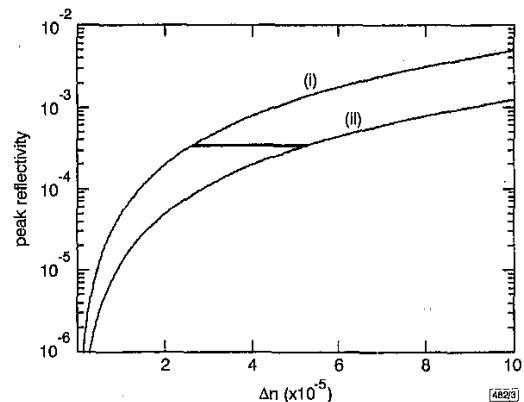


Fig. 3 Computed index change (Δn) for grating written from ± 1 phase mask orders

(i) expected peak reflectivity for grating length 1mm
(ii) expected peak reflectivity for grating length 0.5mm
Horizontal line is measured reflectivity

Using the intensity data for the observed diffraction spots, it was possible to estimate Δn for the strongest grating written in the glass ($m_1 = 1$ and $m_2 = -1$). It was necessary to know the penetration depth of the grating, for that determines the interaction length, and hence the peak reflectivity, for the grating. According to both Othonos and Dyer [5, 6], KrF excimer lasers have the spatial coherence to provide high fringe contrast out to only a few hundred micrometres past the phase mask. We performed exposures with mask/glass separations of 125 and 250μm, each with increasingly faint gratings produced, so at best, it was interpolated that the penetration depth is between 500μm and 1mm. However, by separating the mask and glass, mechanical vibrations as well as fibre heating could have been the largest factor in reducing the grating strength. Shown in Fig. 3 are the theoretical peak reflectivity curves for a grating with two different depths. The left curve assumes a penetration depth of 1mm, and the right curve assumes a penetration depth of 0.5mm. Peak reflectivity for a uniform grating is given by [7]

$$R(\Delta n) = \tanh^2 \left(\frac{\pi \Delta n L}{\lambda_{Bragg}} \right) \quad (3)$$

Note that even if the penetration depth is 0.5mm, the effective grating length (L) that the argon beam interacts with when incident at 27° is 0.17mm. For 1mm penetration, $L = 0.34\text{mm}$. The horizontal line is the measured reflectivity for the first order of the strongest grating. The Δn is expected to lie on this line.

Conclusion: We have demonstrated volume gratings written in BGG31 glass with an excimer laser at 248nm. The glass has neither germanium nor hydrogen to enhance the photosensitivity. The index change inferred was $(3.9 \pm 1.3) \times 10^{-5}$, a reasonable value for this composition of glass. Tests of the transmission properties of these gratings with light coupled into the channel

waveguides have been performed [8], and better than 90% transmission dips at a Bragg wavelength of 1.53 μ m have been obtained.

Acknowledgments: We thank Integrierte Optik GmbH, Waghäusel-Kirrlach, Germany, for providing the BGG31 samples. This work is supported by DARPA and the Office of Naval Research (ONR).

© IEE 1999

Electronics Letters Online No: 19990902

DOI: 10.1049/el:19990902

D. Provenzano, W.K. Marshall and A. Yariv (California Institute of Technology, Mail Stop 128-95, Pasadena, CA 91125, USA)

E-mail: danpro@its.caltech.edu

D.F. Geraghty (NP Photonic Technologies, Tucson, Arizona, USA)

S. Honkanen and N. Peyghambarian (Optical Sciences Center, University of Arizona, USA)

References

- 1 LI, M.J., HONKANEN, S., WANG, W.J., LEONELLI, R., ALBERT, J., and NAJAFI, S.I.: 'Potassium and silver ion-exchanged dual-core glass waveguides with gratings', *Appl. Phys. Lett.*, 1991, **58**, (23), pp. 2607-2609
- 2 NISHII, J.: 'Permanent index changes in Ge-SiO₂ glasses by excimer laser irradiation', *Mat. Sci. Eng.*, 1998, **B54**, (1/2), pp. 1-10
- 3 ROMAN, J.E., and WINICK, K.A.: 'Photowritten gratings in ion-exchanged glass waveguides', *Opt. Lett.*, 1993, **18**, (10), pp. 808-810
- 4 MIYAKE, Y., NISHIKAWA, H., and WATANABE, E.: 'Changes in the optical properties of Ge-doped silica glass during exposure to a KrF excimer laser', *J. Non-Cryst. Solids*, 1997, **222**, pp. 266-271
- 5 OTHONOS, A., and LEE, X.: 'Novel and improved methods of writing Bragg gratings with phase masks', *IEEE Photonics Technol. Lett.*, 1995, **7**, (10), pp. 1183-1185
- 6 DYER, P.E., FARLEY, R.J., and GIEDL, R.: 'Analysis of grating formation with excimer laser irradiated phase masks', *Opt. Commun.*, 1995, **115**, (3/4), pp. 327-334
- 7 OTHONOS, A.: 'Fiber Bragg gratings', *Rev. Sci. Instrum.*, 1997, **68**, (12), pp. 4309-4341
- 8 GERAGHTY, D.F., PROVENZANO, D., HONKANEN, S., MARSHALL, W.K., YARIV, A., and PEYGHAMBARIAN, N.: 'Gratings photowritten in ion-exchanged glass channel waveguides', *Electron. Lett.*, 1999, **35**, (7), pp. 585-587

Multi/demultiplexer consisting of one parent 10GHz-spaced AWG and eight subsidiary 100GHz-spaced AWGs

K. Takada and K. Okamoto

A 320-channel 10GHz-spaced multi/demultiplexer is reported which is realised by connecting eight 100GHz-spaced AWGs in parallel to one 10GHz-spaced AWG. The subsidiary AWGs are conventional 100GHz-spaced AWGs and only one phase-compensated 10GHz-spaced AWG is needed. The configuration is more promising for developing an ultra-dense multi/demultiplexer than that reported previously in which sixteen 10GHz-spaced AWGs were used.

Introduction: Large-scale multi/demultiplexers with narrow channel spacing are attractive for use in increasing the capacity of wavelength division multi/demultiplexing (WDM) systems. We demonstrated a 320-channel 10GHz-spaced multi/demultiplexer consisting of one parent 100GHz-spaced arrayed-waveguide grating (AWG) and 16 subsidiary 10GHz-spaced AWGs [1] thus showing the potential of parallel connection for increasing the number of narrow channels. In practice, however, it is rather difficult to use so many 10GHz-spaced AWGs because a sophisticated phase compensation technique [2] is needed to reduce the crosstalk between the AWGs. We report that the same 320-channel multi/demultiplexer can be constructed by connecting eight conventional 100GHz-spaced AWGs in parallel with only one 10GHz-spaced AWG. This configuration greatly reduces the required number of AWGs.

Configuration: The configuration of our multi/demultiplexer is shown in Fig. 1. It consists of a parent 10GHz-spaced AWG and eight identical 100GHz-spaced 32x32 AWGs, AWG_k ($k = 1, 2, \dots, 8$). The ports on the left and right sides of each AWG are denoted as the input and output ports, respectively, and they are numbered 1, 2, ... from top to bottom. Input port 8 of the parent AWG was used as the multi/demultiplexer input port, and every output port was connected to either the input or output port of AWG_k through optical fibres. Output ports 2k-1 was connected to input port 16 of AWG_k through optical fibres. Output ports 2k ($k = 1, \dots, 8$) were connected to output ports 20, 20, 17, 19, 16, 16, 13, and 18 of AWG_k ($k = 1, \dots, 8$), respectively, through optical fibres.

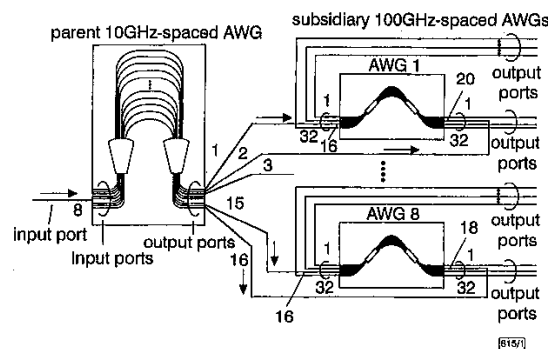


Fig. 1 Schematic diagram of 320-channel multi/demultiplexer

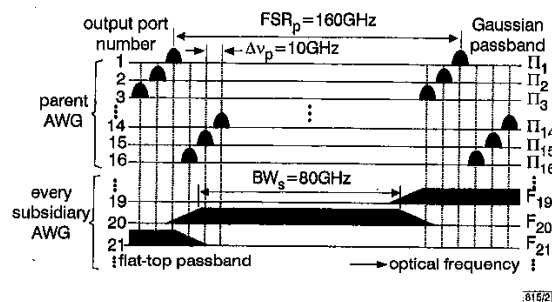


Fig. 2 Optical frequency relation between passbands of parent AWG and subsidiary AWG with input ports 8 and 16 for light incidence

Gaussian passbands obtained at different diffraction orders from output port j ($j = 1, 2, \dots, 16$) of the parent AWG, input port 8 of which is used for light incidence, appear repeatedly at $FSR_p = 160$ GHz intervals and the group is named Π_j . Changing the output port shifts the group by an integer multiple of $\Delta\nu_p = 10$ GHz, as shown in the upper part of Fig. 2. Flat-top passbands F_m ($m = 1, 2, \dots, N_s$) obtained from all $N_s = 32$ output ports of AWG_k, input port 16 of which is used for light incidence, have a bandwidth of $BW_s = 80$ GHz and are arranged at $\Delta\nu_s = 100$ GHz intervals, as shown in the lower part of the Figure. Each passband is used to block unwanted passbands in Π_j .

Principle of operation: The passbands obtained from N_s output ports of AWG_k in the multi/demultiplexer are given by multiplying Π_{2k-1} with F_m ($m = 1, 2, \dots, N_s$). Under the condition that the bandwidth $BW_s < FSR_p$, one Gaussian passband at most in Π_{2k-1} is allowed to pass through every F_m . The number of unblocked and available passbands from AWG_k is $N_s \times \Delta\nu_s / FSR_p = 20$ and thus a group of 160 Gaussian passbands is obtained from all the output ports of AWG_k ($k = 1, 2, \dots, 8$). Since the cyclic condition of $N_s \times \Delta\nu_s = FSR_s$ is approximately satisfied for AWG_k, the free spectral range of which is FSR_s , almost the same passbands as F_m ($m = 1, 2, \dots, N_s$) are obtained from its N_s input ports when an output port other than 16 is used for light incidence. Therefore, another group of 160 passbands is obtained from all input ports of AWG_k ($k = 1, 2, \dots, 8$). The bandwidth and cyclic conditions ensure that the two groups are combined to give 320 Gaussian passbands arranged at $\Delta\nu_p$ intervals.

There is at least one output port m in AWG_k for every value of k , such as output port 20 of AWG₁ as shown in Fig. 2, the pass-